AGU PUBLICATIONS

JGR

Journal of Geophysical Research: Space Physics

RESEARCH ARTICLE
10.1002/2015JA021950

Key Points:
- Describes a previously unrecognized source of dawn-dusk asymmetry in rapidly rotating magnetospheres
- Asymmetry arises from the different rates of plasma expansion and contraction along flux tubes prenoon and postnoon
- The mechanism explains Saturn's noon-midnight E field and may produce analogous effects at Jupiter

Correspondence to:
X. Jia,
xzjia@umich.edu

Citation:
Jia, X., and M. G. Kivelson (2016), Dawn-dusk asymmetries in rotating magnetospheres: Lessons from modeling Saturn, *J. Geophys. Res. Space Physics*, *121*, 1413–1424, doi:10.1002/2015JA021950.

Received 24 SEP 2015
Accepted 4 FEB 2016
Accepted article online 8 FEB 2016
Published online 27 FEB 2016

Dawn-dusk asymmetries in rotating magnetospheres: Lessons from modeling Saturn

Xianzhe Jia[1] and Margaret G. Kivelson[1,2]

[1]Department of Climate and Space Sciences and Engineering, University of Michigan, Ann Arbor, Michigan, USA, [2]Department of Earth, Planetary, and Space Sciences, University of California, Los Angeles, California, USA

Abstract Spacecraft measurements reveal perplexing dawn-dusk asymmetries of field and plasma properties in the magnetospheres of Saturn and Jupiter. Here we describe a previously unrecognized source of dawn-dusk asymmetry in a rapidly rotating magnetosphere. We analyze two magnetohydrodynamic simulations, focusing on how flows along and across the field vary with local time in Saturn's dayside magnetosphere. As plasma rotates from dawn to noon on a dipolarizing flux tube, it flows away from the equator along the flux tube at roughly half of the sound speed (C_s), the maximum speed at which a bulk plasma can flow along a flux tube into a lower pressure region. As plasma rotates from noon to dusk on a stretching flux tube, the field-aligned component of its centripetal acceleration decreases and it flows back toward the equator at speeds typically smaller than $\frac{1}{2}C_s$. Correspondingly, the plasma sheet remains far thicker and the field less stretched in the afternoon than in the morning. Different radial force balance in the morning and afternoon sectors produce asymmetry in the plasma sheet thickness and a net dusk-to-dawn flow inside of $L = 15$ or equivalently, a large-scale electric field (**E**) oriented from postnoon to premidnight, as reported from observations. Morning-afternoon asymmetry analogous to that found at Saturn has been observed at Jupiter, and a noon-midnight component of **E** cannot be ruled out.

1. Introduction

Earth's magnetosphere is not fully symmetric about the noon-midnight meridian. Asymmetries arise because of the effects of rotation, which carries plasma sunward on the morning side and antisunward on the evening side, and because hot protons injected on the nightside move toward dusk through the action of gradient and curvature drift. Resulting asymmetries include a slight duskward displacement of the plasmapause and an asymmetric ring current, more intense near dusk. These asymmetries are well understood.

The magnetospheres of Jupiter and Saturn also manifest dawn-dusk asymmetries. In Jupiter's inner magnetosphere, the Io plasma torus is brighter on the dusk side than on the dawn side, a feature that has been explained by postulating a dawn-dusk electric field that shifts the torus slightly toward dawn and concurrently heats the plasma more on the dusk side than the dawn side [*Barbosa and Kivelson*, 1983; *Ip and Goertz*, 1983].

At the outer planets, flows, although subcorotational, are predominantly azimuthal through much of the equatorial magnetospheres of both Jupiter [*Krupp et al.*, 2001] and Saturn [*Holmberg et al.*, 2012; *Kane et al.*, 2014; *Sakai et al.*, 2013; *Thomsen et al.*, 2010, 2012; *Wilson et al.*, 2009]. These flows may produce dawn-dusk asymmetries, especially near the outer boundaries where interaction with magnetosheath flow implies a radial gradient of the azimuthal flow larger near dawn than near dusk, although the postulated increased probability of Kelvin-Helmholtz instabilities near dawn [*Desroche et al.*, 2012, 2013] is the opposite of what has been observed at Saturn [*Delamere et al.*, 2013].

Additional asymmetries have been identified in the structure of Jupiter's equatorial plasma beyond ~20 R_J (R_J is the radius of Jupiter). Both the field configuration and the distribution of plasma along the field change markedly with local time (LT). The region of significant plasma density is far thicker at dusk than at dawn. In the postmidnight to midmorning sector, magnetospheric plasma is concentrated near the centrifugal equator [*Hill et al.*, 1974], and the outward force of pressure gradients and the effects of rotating dense plasma stretch the field into a tail-like configuration [*Mauk et al.*, 1985; *Mauk and Krimigis*, 1987]. As local time increases from noon to dusk, thickening of the plasma sheet is seen in both data [*Lanzerotti et al.*, 1992; *Khurana et al.*, 2004; *Kivelson and Southwood*, 2005] and global MHD models such as that of *Fukazawa et al.* [2005]. The plasma sheet is typically of order 2 R_J thick postmidnight and around to midmorning and becomes as thick as ~20 R_J near dusk as evident

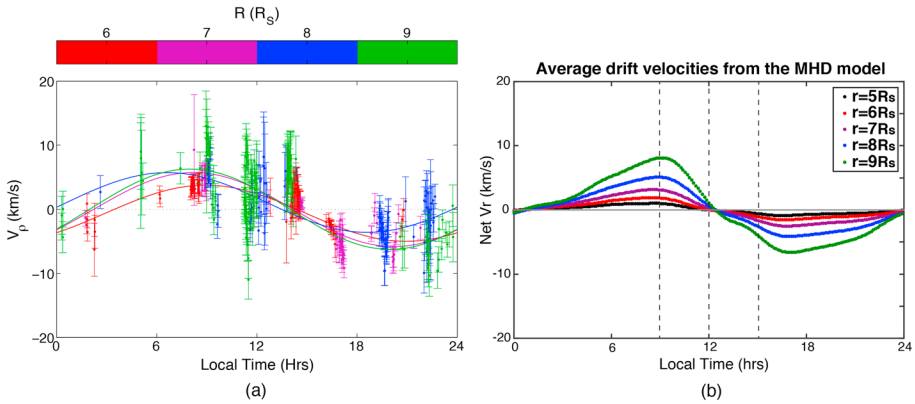

Figure 1. (a) From *Wilson et al*. [2013], their Figure 4. Average radial (cylindrical) drift velocity at different radial distances as indicated by the color bar at the top. (b) Average radial drift velocities from a magnetohydrodynamic model discussed in this paper with the same color/distance correspondence and black for flow at $r = 5\ R_S$. Dotted vertical lines have been added at 09, 12, and 15 LT to call attention to the change of the direction of the radial component of the flow between 3 h prenoon, at noon, and 3 h postnoon.

from the ~10 h periodicity of the electron and ion fluxes measured at high latitudes by Ulysses on its outbound pass [*Lanzerotti et al*., 1992]. Correspondingly, the magnetic field is more dipolar near dusk than near dawn [*Khurana et al*., 2004; *Kivelson and Southwood*, 2005]. It seems that a similar but smaller degree of asymmetry exists at Saturn [*Arridge et al*., 2015]. Although the source of these dawn-dusk asymmetries has not been identified clearly, it has been suggested that the structure results in part from the effects of magnetopause confinement coupled with LT variation of the acceleration arising from the rotation of the plasma, often described as centrifugal force [*Kivelson and Southwood*, 2005; *Vogt et al*., 2014].

At Saturn, an electric field oriented roughly from noon to midnight and corresponding to a net radially inward flow on the afternoon side and radially outward flow on the morning side has been identified in the equatorial magnetosphere inside of $10\ R_S$ ($R_S = 60{,}268$ km is Saturn's radius) [*Thomsen et al*., 2012; *Wilson et al*., 2013; *Andriopoulou et al*., 2012, 2014]. Figure 1a from *Wilson et al*. [2013] shows the effect of the field on the flow velocity, revealing an asymmetry of the radial flow about the noon-midnight meridian. Such a flow pattern was not anticipated in advance of the measurements. There is a slight morning-evening asymmetry in the magnetopause location [*Kivelson and Jia*, 2014; *Pilkington et al*., 2015], an asymmetry that is internally generated and is present even when external forces impose no asymmetry. The fit provided by *Kivelson and Jia* [2014] indicates that the magnetopause lies ~5% farther out at 09 than at 15 LT, an asymmetry small enough that one might expect outward radial flow close to symmetric about noon. Yet this is not the case. The noon-midnight electric field identified inside of $10\ R_S$ implies morning-afternoon asymmetry of radial flow deep within the magnetosphere. *Thomsen et al*. [2012] say "The source of such an electric field remains a puzzle, but whatever the source, it appears to be a dominant factor in the circulation of plasma in Saturn's inner magnetosphere," *Wilson et al*. [2013] state that "the origin of the electric field remains a mystery," and *Andriopoulou et al*. [2014] concur, stating that "the … presence of a convective electric field in Saturn's inner and middle magnetosphere, with an average pointing approximately towards midnight … is one of the most puzzling findings by the Cassini spacecraft."

Our purpose in this paper is to account for some of the morning-evening asymmetries of Saturn's magnetosphere by analyzing magnetohydrodynamic (MHD) simulations previously developed for other purposes. The phenomena described appear on scales large compared with characteristic kinetic effects, and thus, the MHD limit is expected to represent the relevant properties of the system appropriately. We use the simulations to identify the dynamical response of the plasma of Saturn as it rotates from the morning to the evening side of the magnetosphere. In particular, we examine the intimate link between field configuration and the effects of azimuthal flows on plasma properties. We use two different model runs. In one from which we extract most of the results, no internal current sources are imposed from the ionosphere [*Jia et al*., 2012a]. We then show that another model run in which a rotating system of field-aligned currents is driven from the southern ionosphere [*Jia et al*., 2012b] displays similar asymmetries.

2. The Simulation

This investigation of flows in Saturn's magnetosphere is based on outputs from the global MHD model, BATSRUS (Block Adaptive Tree Solar-wind Roe-type Upwind Scheme), described by *Powell et al*. [1999], *Gombosi et al*. [2002], and *Toth et al*. [2012], coupled to the effective ionosphere with an ionosphere electrodynamics solver [*Ridley et al*., 2004]. The runs on which this work is based have been described in detail by *Jia et al*. [2012a, 2012b] and *Jia and Kivelson* [2012]. Of special importance to this paper are the following features:

1. The planetary magnetic field is represented as a centered dipole aligned with the spin axis (*z* axis).
2. The solar wind is taken to flow with a velocity of 400 km/s at right angles to the spin axis. The solar wind plasma density is set to 0.05 amu/cm^3, and its temperature is set to 20 eV. The interplanetary magnetic field of magnitude 0.5 nT is oriented southward, thus minimizing reconnection with the planetary magnetic field. These solar wind properties are kept fixed throughout the times from which we extract output from the two simulations. The inner boundary of the simulation is a sphere at 3 R_S. The magnetosphere is coupled to the ionosphere by mapping potential contours along the magnetic field from a sphere at 4 R_S and thereafter mapping the modified ionospheric potential contours back into the magnetosphere. Ionospheric and magnetospheric flows are, therefore, strongly coupled, and magnetospheric drag slows the ionosphere.
3. In the simulation of *Jia et al*. [2012b], which we designate as "with vortex," the ionosphere is perturbed by a pair of flow vortices centered at 70° latitude in the south. The rotating vortical flows were imposed as a way to drive field-aligned currents from one ionosphere to the other [*Southwood and Kivelson*, 2007; *Andrews et al*., 2008] and into the magnetosphere. They rotate rigidly at the nominal period of modulation of the Saturn kilometric radiation [*Lecacheux et al*., 1997; *Galopeau and Lecacheux*, 2000; *Gurnett et al*., 2005; *Kurth et al*., 2007, 2008; *Lamy*, 2011] relevant to the early part of the Cassini mission near southern summer solstice. In order to mimic the effect of asymmetric solar illumination on ionospheric conductance, we specify a uniform conductance of 3 S for the southern ionosphere and 1 S for the northern ionosphere. In the simulation of *Jia et al*. [2012a], there is no internal source of periodicity, and we refer to it as "without vortex." In this simulation, we assume a uniform conductance of 0.5 S for both ionospheres.
4. Neutral sources, representing the material originating in the plumes of Enceladus and the atmosphere of Titan, are incorporated by including axisymmetric disc-like distributions of neutrals [*Hansen et al*., 2005], one representing water group molecules (*W*) with the ion production rate peaked at ~5.35 R_S [*Richardson et al*., 1998] and one corresponding to nitrogen atoms (*N*) with the ionization production rate peaked around Titan's orbit at ~20 R_S. Recent Cassini observations show little evidence of N^+ production from Titan but rather suggest that Titan is an important source of H_2^+ [*Thomsen et al*., 2010]. The relatively low production rates of these species suggest that our simulation results would be little affected by changing the neutral source model. Source and loss terms in the equations of the simulation represent ionization, charge exchange, and recombination. Charge exchange does not contribute to the mass balance but changes the temperature and momentum. The process is incorporated based on the results of *Richardson et al*. [1998] that provide information about the oxygen neutral density (peaks at ~ 4 R_S) and the reaction rate. The total charge exchange rate used is ~ 70 kg/s. In the simulation with vortices, contributions are normalized to give a net mass loading rate of $\sim 6\times10^{27}$/s for W^+ and $\sim 5\times10^{25}$/s for N^+, corresponding to a total mass loading rate of plasma of ~170 kg/s assuming an average mass of 16.6 amu for W^+ and 14 amu for N^+, which are within the range of estimated rates. The simulation without vortices uses a smaller mass loading rate (85 kg/s), a difference that decreases the standoff distance of the magnetopause but is not expected to produce significant changes of the dynamics of the system.

3. Forces Acting on the Plasma

The global MHD simulation of *Jia et al*. [2012a] was designed to investigate how Saturn's magnetosphere responds to different solar wind drivers. During the first 100 h of the run, the solar wind dynamic pressure is set to 0.02 nPa and the interplanetary magnetic field is southward oriented. Reconnection with the solar wind is not significant, and the magnetosphere is nearly quiescent as expected for such conditions. This quasi steady state interval is the portion of the run that we examine with the objective of understanding the mechanisms that produce dawn-dusk asymmetries and, in particular, the observed noon-midnight electric

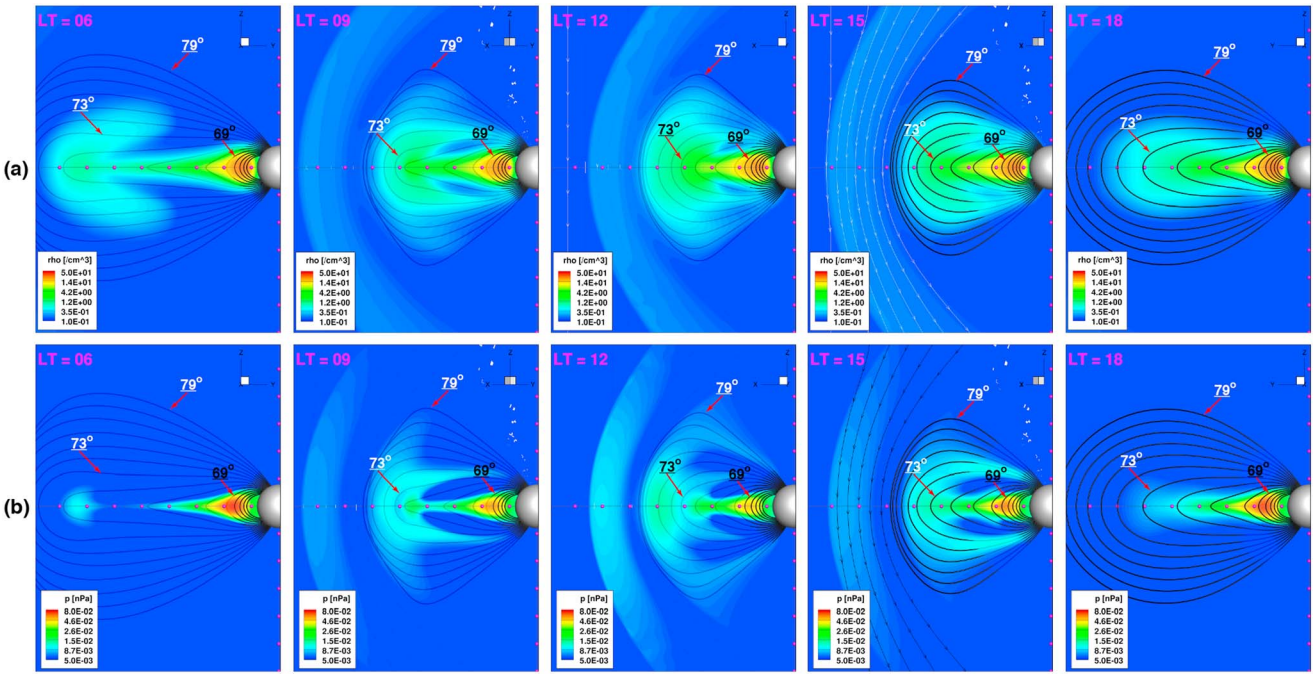

Figure 2. From the simulation of *Jia et al*. [2012b]. (a) Density (rho, in #/cm^3) and (b) Thermal pressure (p in nPa) represented by color in the 06, 09, 12, 15, and 18 LT meridian planes. Field lines emerging from 79° and lower latitudes, separated by 1°, are projected into the meridian planes illustrated. Heavier black lines show where the field lines lie in the meridian plane or ahead of it in the sense of rotation, and lighter lines show lagging field lines. Additional magnetosheath field lines are shown. Magenta circles are separated by 5 R_S.

field (**E**). We start by comparing key properties of the field and plasma in five different local time sectors: 06, 09, 12, 15, and 18 LT, averaged over five rotation cycles. Our objective is to identify the processes that account for a noon-midnight $\mathbf{E} = -\mathbf{v}\times\mathbf{B}$ electric field. Noting that the plasma flows associated with a given **E** vary in magnitude inversely with **B**, becoming exceedingly small at small radial distances, we consider initially the near-equatorial plasma in regions beyond $10\,R_S$ where $B \lesssim 20$ nT and typical flow perturbations are $> 10\,\mathrm{km\,s^{-1}}$ [*Wilson et al*., 2013].

The density and thermal pressure in five meridian planes centered at noon is shown in Figure 2. The plots include projections into these planes of field lines originating in the ionosphere at 79° (approximately the last closed field line on the dayside) and successively lower latitudes separated by 1° down to 65° and some magnetosheath field lines. The field lines above 73° invariant latitude that cross the equator beyond $20\,R_S$ and are strongly modified by magnetopause currents have similar form in the selected meridian planes, all being close to dipolar near the equator. Plasma fills these flux tubes to large distances above the equator. Lower invariant latitude field lines down to ~69° (crossing the equator near $9\,R_S$) are quite tail-like near the equator, with considerably more stretching prenoon than postnoon. The plasma pressure on these flux tubes falls off rapidly with distance from the equator and the field structure and plasma distributions vary significantly with LT. This range of invariant latitudes (~69° to ~73°) is particularly useful in revealing the dynamical responses of the plasma and field associated with rotation from prenoon to postnoon.

We start by considering stress balance in the plasma. The governing equation is the momentum equation, $\rho\,(\mathbf{u}\cdot\nabla\mathbf{u}) = \mathscr{F}$, where ρ is the mass density, **u** (u_r, u_ϕ, u_z) is the bulk flow velocity, and $\mathscr{F}$ is the force density. Forces acting to move plasma inward are the pressure gradient force $(-\nabla p)$ wherever the pressure gradient is positive outward and the $\mathbf{j}\times\mathbf{B}$ force. Here p is the thermal pressure, **j** is the current density, and **B** is the magnetic field. Acting to move plasma outward is the pressure gradient force wherever the gradient is positive inward. In addition, plasma rotating around the planet experiences inward radial acceleration arising from the term proportional to $(\mathbf{u}\cdot\nabla\mathbf{u})$ in the momentum equation. In cylindrical coordinates, the axial radial component of this acceleration is $\left[u_r\frac{\partial}{\partial r}u_r + u_\phi\frac{\partial}{r\partial\phi}u_r + u_z\frac{\partial}{\partial z}u_r - \frac{u_\phi^2}{r}\right]$. We are interested in the variation of the system with ϕ, so the second term is of interest. In both Jupiter's and Saturn's magnetospheres, the azimuthal

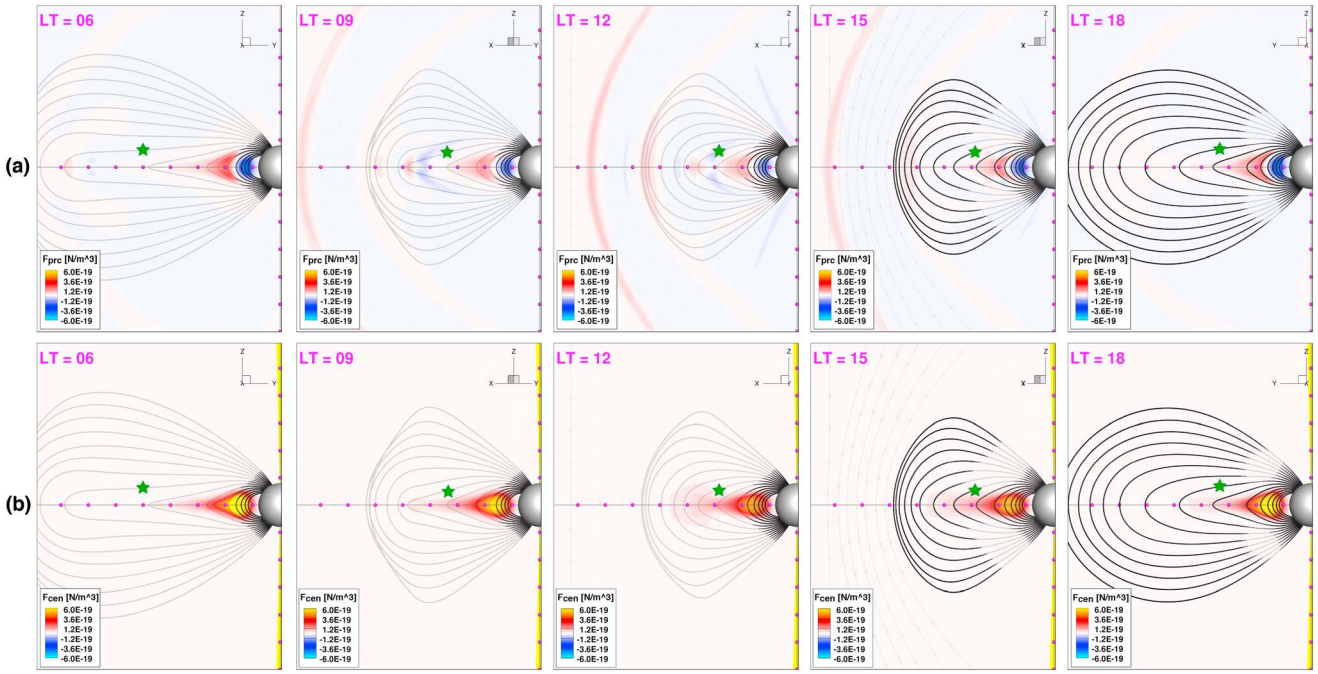

Figure 3. Cylindrical radial component (in N/m^3) arising from (a) pressure gradients (F_{prc}) and (b) the centripetal term (F_{cen}) at three different local times. From left to right these are 06, 09, 12, 15, and 18 LT. Outward forces are plotted in red. Inward forces are plotted in blue. Magenta circles on the axes are separated by 5 R_S. As in Figure 2, field lines emerging from 65° to 79° latitude are shown at the selected local times. Green stars identify 72° invariant latitude field lines.

velocity is at least an order of magnitude larger than the velocity components in the radial direction and parallel to the spin axis, and the velocities change slowly in all three directions. Thus, the first and third terms are small compared with the other terms, so we set

$$(\mathbf{u}\cdot\nabla\mathbf{u})_r \cong u_\phi \frac{\partial}{r\partial\phi} u_r - u_\phi^2/r \tag{1}$$

The (cylindrical) radial component of the momentum equation can then be approximated as

$$\rho u_\phi \frac{\partial}{r\partial\phi} u_r \cong -\nabla_r p + \rho u_\phi^2/r + (\mathbf{j}\times\mathbf{B})_r \tag{2}$$

where the second term on the right side is colloquially referred to as the centrifugal force. Recognizing its origin in equation (1), where it represents inward acceleration of the rotating mass density, we refer to it as the centripetal term, noting that in equation (2) it is always positive.

Figure 3 shows the cylindrical radial components of the pressure gradient force (both positive and negative) and the centripetal term (always positive) at the different LTs. The outward centripetal term is stronger in the morning sector (06 and 09 LT) than in the comparable evening sector (15 and 18 LT). Figure 4 shows the cylindrical radial component of the $\mathbf{j}\times\mathbf{B}$ force, which is everywhere inward and particularly large in parts of the postnoon sector. The figure also shows the full right-hand side of equation (2) in the selected meridian planes.

In Figures 3 and 4, the black curves represent projections into meridian planes of field lines from fixed latitudes in the ionosphere starting from 79° and successively lower latitudes with 1° separations. Thinner lines indicate that the field lines lag the meridian plane in the sense of rotation, and thicker lines indicate that the field lines are in the meridian plane or lead it. The LT dependence of field line bending out of meridian planes is made more evident in Figure 5, which shows (blue circles) the equatorial crossing positions of the field lines originating in the ionosphere at 09, 12, and 15 LT at latitudes separated by 1° starting at 65°. In the morning sector, field lines lag at all invariant latitudes >74° (equatorial crossing at ~12 R_S), with the lag extreme (>1 h of LT) beyond 74° invariant latitude (~30 R_S). At noon, the lag is present at invariant latitude > 70° (~12 R_S) and becomes extreme beyond 76° invariant latitude (>28 R_S). In the afternoon sector, the field lines lead slightly near 72° invariant latitude (between 15 and 20 R_S); the lead becomes substantial beyond 72° invariant latitude (~25 R_S).

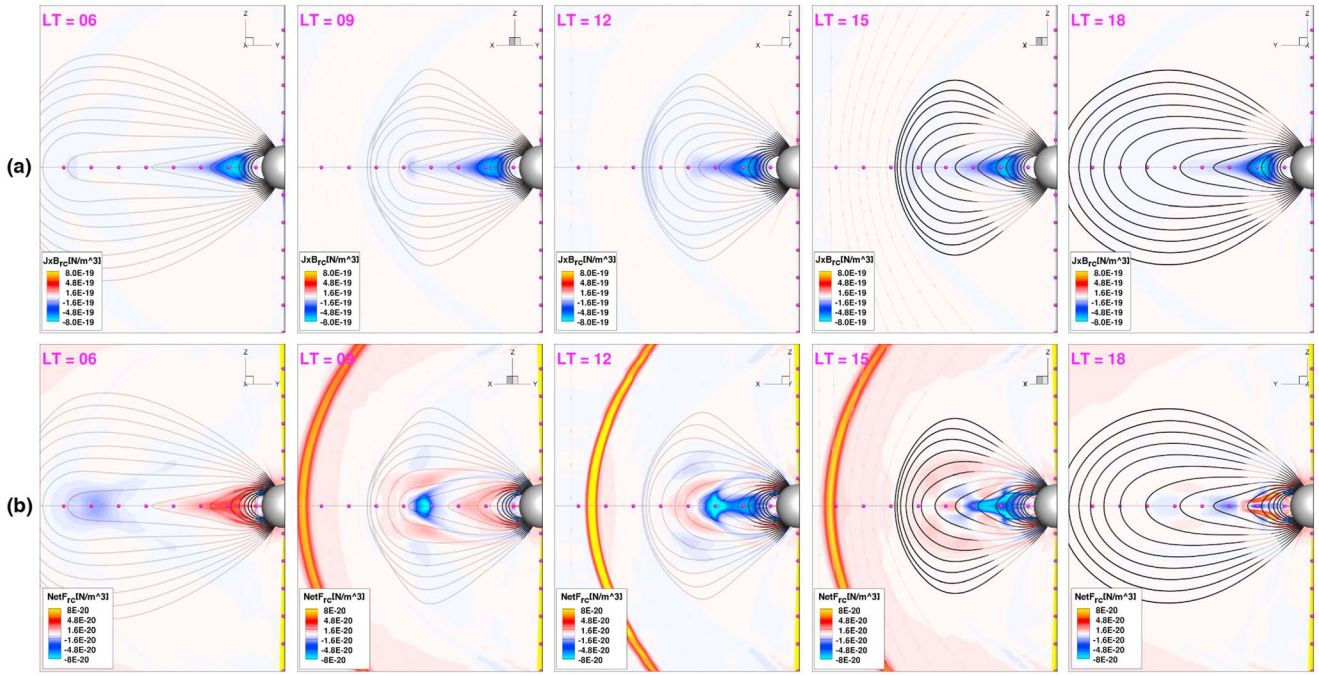

Figure 4. As for Figure 3, the cylindrical radial component of (a) the $\mathbf{j} \times \mathbf{B}$ force density (JxB_{rc} in N/m^3) at five local times centered at noon and (b) the sum of the contributions to the right side of equation (2) (NetF_{rc} in N/m^3).

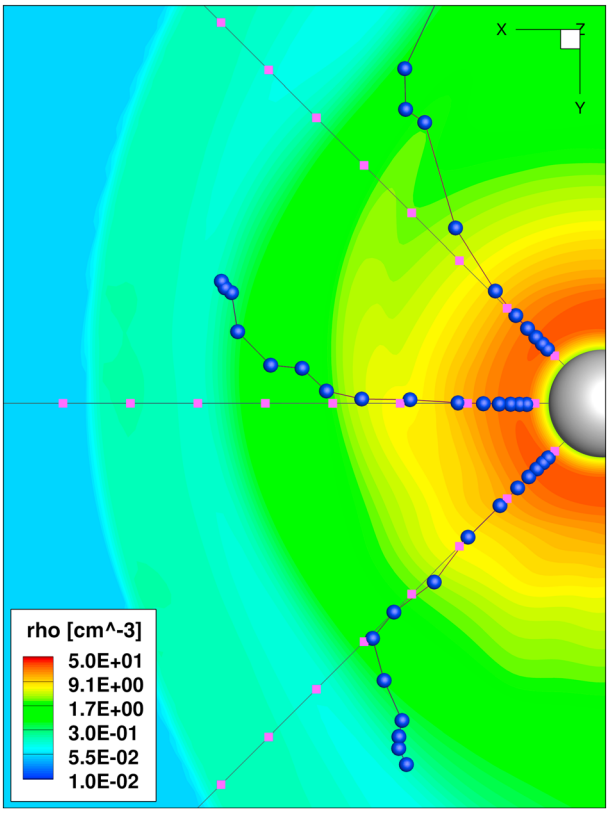

Figure 5. Equatorial crossings of field lines that start in the ionosphere at different latitudes in the 09, 12, and 15 LT meridian planes. At 09 LT, the blue circles correspond to 65° to 74° invariant latitude. At 12 and 15 LT the blue circles correspond to 65° to 79° invariant latitude. The background color shows the equatorial plasma density.

The field lines drawn in Figures 3 and 4 illustrate another important feature of the LT asymmetry. The field lines that emerge from the ionosphere at 09 LT are far more stretched than those that emerge at 15 LT. For example, the field line that emerges at 72° (identified by stars placed on the plots in the top row of Figure 3) crosses the equator at ~24 R_S near 09 LT but extends only to ~18 R_S at both 12 and 15 LT. The crossing points at 06 LT (39 R_S) and 18 LT (24 R_S) are even more asymmetric. These equatorial crossing distances confirm that the dipolarization of flux tubes that occurs beyond the noon meridian does not reverse as the flux tubes rotate into the postnoon sector. After having discussed other features of the simulation, we will return to this aspect of the asymmetry, which is closely linked to the thickening of the plasma sheet in the afternoon sector.

4. Local Time Variation of Forces

The force that dominates the radial displacement of plasma differs on the morning and evening sides of the magnetosphere. Consider the total force near the equator shown in Figure 4b. It is striking that inside of ~17 R_S (which includes the region in which a noon-midnight electric field has been identified), the sum of the terms governing $\rho u_\phi \frac{\partial}{r\partial\phi} u_r$ is outward at 06 and 09 LT, inward at 15 LT, and mostly inward near the equator at 18 LT. Outward acceleration in the prenoon sector and inward acceleration postnoon are consistent with the different directions of radial flow in the morning and evening LT sectors shown in Figure 1. Within 17 R_S, the pressure gradient force is weak and varies little with LT. The strong (outward) centripetal term dominates in the morning sector (see Figure 3b) and results in outward flow. The inward $\mathbf{j}\times\mathbf{B}$ force dominates in much of the afternoon sector and produces inward acceleration sufficient to reverse the direction of radial flow.

The different directions of radial flow in the meridian planes symmetric about noon are consistent with the shift in the principal force acting on the near-equatorial plasma prenoon and postnoon. But why are the forces asymmetric? Consideration of forces acting along the field gives insight. In Figure 6 we plot the contributions to radial acceleration parallel to **B** arising from the pressure gradient force and the centripetal term; the $\mathbf{j}\times\mathbf{B}$ force does not act along the field. The field-aligned component of the centripetal term is proportional to $\hat{\mathbf{b}}\cdot\hat{\mathbf{r}}$, where $\hat{\mathbf{b}}$ is a unit vector along the background field, **B**, and $\hat{\mathbf{r}}$ is a unit vector radially outward from the rotation axis. Between $L\sim7$ and 15 and near the equator, the net parallel force is directed toward the equator in the morning but is directed away from the equator at 12 LT and continues to be so directed at 15 LT, reversing direction again at 18 LT. The change of the direction of the field-aligned force is consistent with the different field configurations prenoon, at noon, and postnoon. In the 09 LT meridian plane, the field is significantly stretched in the middle magnetosphere, implying relatively large values of $\hat{\mathbf{b}}\cdot\hat{\mathbf{r}}$ to within a few degrees of the equator. As a flux tube rotates from 09 LT to 12 LT, the distance to the magnetopause decreases, and in most of the meridian plane, the field configuration becomes increasingly dipolar. Although the centripetal term is effective in confining plasma near the equator in a stretched field, for which $\hat{\mathbf{b}}\cdot\hat{\mathbf{r}}$ is nonnegligible over a significant part of the flux tube, it is far less effective in a dipolar field for which $\hat{\mathbf{b}}\cdot\hat{\mathbf{r}}$ remains small over a considerable range of latitudes about the equator. Thus, the plasma, confined to very low latitudes near 09 LT, expands to fill the flux tube to higher latitude as it rotates to noon and becomes more dipolar. The expansion of plasma on flux tubes crossing the equator between 10 and 17 R_S as they rotate from 09 LT to 12 LT can be identified in the density plots of Figure 2. For example, one can follow the low density boundary (dark blue) on the field line at 72° invariant latitude from 09 LT, where it is located ~18 R_S from the spin axis, to 12 LT, where it is located at ~13 R_S from the spin axis.

As the flux tubes rotate from 12 LT to 15 LT, they do not stretch back to their configurations at 09 LT. This is the aspect of the system that must be accounted for. We suggest that the asymmetry develops because plasma expansion and contraction along a flux tube in a rotating system is not symmetric about noon, a feature of a rotating system that has not previously been considered. As plasma rotates through the morning quadrant, e.g., from 06 LT to 12 LT, the field becomes increasingly dipolar in configuration as a result of magnetopause confinement and associated compression. The compression affects the equatorial crossing points of flux tubes deep into the middle magnetosphere. (The inward displacement of the equatorial crossing of field lines at invariant latitudes >69° can be seen in Figure 2, for example.) Because the $\mathbf{j}\times\mathbf{B}$ force has no field-aligned component, it is the combination of the pressure gradient force and the centripetal term that determines the distribution of plasma along the flux tube. Dipolarization reduces the outward-directed

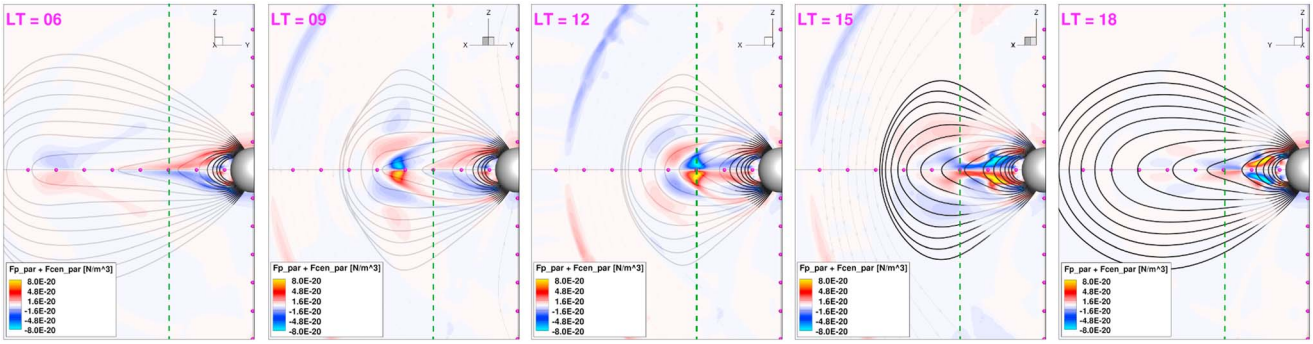

Figure 6. The sum of the field-aligned components of the pressure gradient and the centripetal term in the 06, 09, 12, 15, and 18 LT planes in N/m^3. Color bars range from negative to positive values, with positive values implying that the force is in the direction of the field (i.e., toward the equator in the north). Because the radial component of the field reverses across the equator, positive values of the net force are equatorward above the equator and away from the equator below the equator. Green vertical lines are drawn at 15 R_S from the spin axis. At 09 LT, the net force is equatorward on L shells between 7 and 15, but at 15 LT, the net force in the same L range is mostly away from the equator.

field-aligned component of the centripetal term and the equator-directed pressure gradient drives expansion of plasma along the flux tube. In the absence of other effects, plasma expands along a flux tube behind a slow mode front that moves away from the equator at the sound speed, C_s, but at Saturn the actual speed is reduced by the field-aligned component of the centripetal term. As flux tubes rotate into the afternoon sector, the plasma can return to the equator no faster than the rate to which it can be accelerated by changes of the field-aligned component of centripetal acceleration. This upper limit is not achieved because the pressure gradient force continues to resist compression. One can estimate the maximum rates of expansion away from the equator prenoon and compression postnoon from the plots of Figure 7. Near 10 R_S, for example, the sound speed is approximately 50 km s^{-1}. Rotation from 09 LT to noon requires close to 1.7 h (on average at ~80% of rigid corotation speed in the simulation), during which time flow at C_s would displace a front by ~5 R_S along the flux tube. The centripetal acceleration near 10 R_S at noon is close to 6 m s^{-2} or 1.3 R_S h^{-2}, implying that in approximately 1.7 h required for a flux tube to rotate from noon to 15 LT a front can move no more than ~1.9 R_S. These estimates give upper and lower bounds but suffice to demonstrate that motion of plasma along a flux tube differs in the morning and the afternoon because of the different

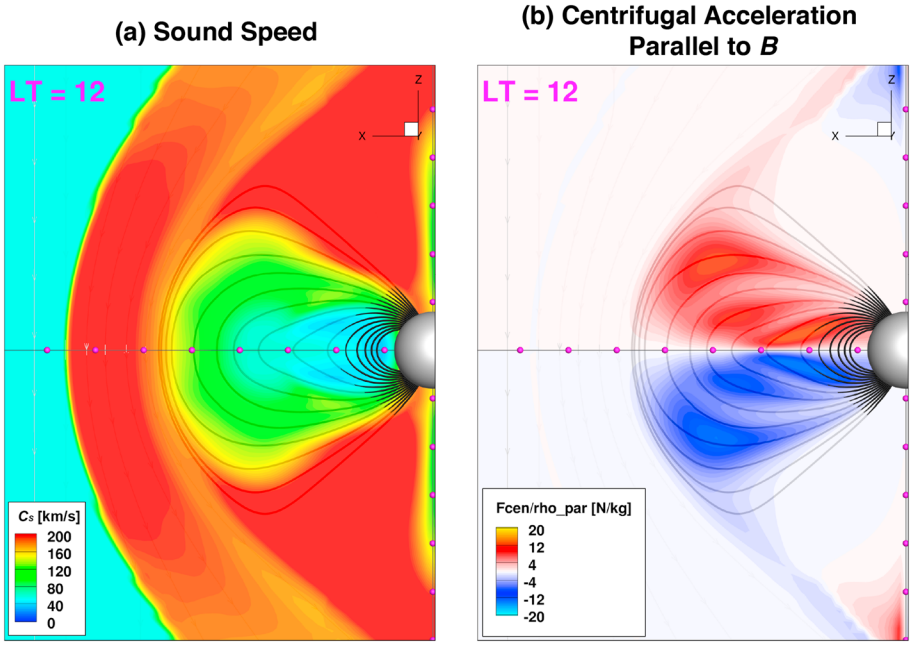

Figure 7. (a) Sound speed (C_s) in km/s and (b) the negative of the centripetal acceleration (component of u_ϕ^2/r parallel to **B**) in m/s^2 in the 12 LT meridian plane.

physical processes that dominate expansion and contraction. The plasma cannot easily return to its prenoon near-equatorial confinement as it rotates into the afternoon sector.

Different distributions of plasma along a flux tube affect the configuration of the field. Stretching occurs if the radially outward forces fall off rapidly with increasing latitude along the flux tube. In the absence of anisotropy, mass must be concentrated at the equator in order to produce the increased magnetic curvature force present at low latitudes in a stretched field configuration. If the plasma extends to significant distances off the equator, field curvature near the equator decreases. The slow return of mass density to the equator as the flux tube rotates through the afternoon sector accounts for both a thick plasma sheet on the afternoon side of the magnetosphere and a field configuration that remains quasi-dipolar as it rotates through the afternoon sector.

5. Asymmetry of Flow and the Electric Field in the Middle Magnetosphere: Simulation

Measurements that imply a noon-midnight electric field have been made inside of 10 R_S [*Thomsen et al*., 2012; *Wilson et al*., 2013; *Andriopoulou et al*., 2012, 2014]. A noon-midnight electric field implies a dusk to dawn flow whose radial component is outward in the morning sector and inward in the afternoon sector. In the simulation, the flow asymmetries become clearer at distances slightly larger than 10 R_S, so we focus initially on simulation results in the 69° to 71° invariant latitude range (equatorial crossing from ~9 to >15 R_S) where key features of the simulation can be more easily identified in the figures. At 09 LT, the field in this range of invariant latitudes is somewhat stretched and outward centripetal terms are not fully balanced by the sum of pressure gradient and $\mathbf{j}\times\mathbf{B}$ forces, as can be seen in Figure 4b. The imbalance is feeble but sufficient to produce outward radial flow. At 15 LT, the imbalance is significant and the net force is inward directed. The radial component of the flow is inward.

In Figure 8 we show in color the radial component of the flow velocity in the equatorial plane at all local times extracted from two simulations, the one without an imposed system of rotating vortices in the ionosphere [*Jia et al*., 2012a] that has been used to provide the other plots of this paper and the one with vortices [*Jia et al*., 2012b]. Black arrows show the orientation and the magnitude of the electric field (obtained from $\mathbf{E}=-\mathbf{v}\times\mathbf{B}$) after subtraction of the radial electric field corresponding to the azimuthal component of the flow averaged over all local times at a given radial distance. Figure 8 shows that the flow in the simulation is consistent with a roughly noon-midnight electric field everywhere inside of ~15 R_S. It is notable that inside of 15 R_S the electric field vectors differ little between the two models, revealing that in this part of the magnetosphere, the morning-afternoon asymmetry does not arise as a result of rotational modulation. As anticipated from the force analysis, there is net outward radial flow in the prenoon sector and net inward radial flow in the postnoon sector. Figure 1b shows the radial flow velocity from the simulation as a function of LT at a range of radial distances between 5 and 9 R_S, the region in which the flow has been identified in data. Note that both the amplitude and the LT dependence of the radial velocity in the simulation are close to those shown in Figure 1a from data analysis by *Wilson et al*. [2013]. The similarity between the simulated flows and those observed gives us confidence that the irreversibility of plasma expansion and contraction along flux tubes is the source of the asymmetry.

Although the flows in the simulations with and without vortex differ little in the region inside of 15 R_S (75° invariant latitude), within which the noon-midnight electric field has been identified in data, they differ considerably beyond ~15 R_S. In the simulation without vortices, at distances beyond 15 R_S the flow is largely inward in the morning sector, where magnetopause confinement dictates inward motion, and largely outward in the postnoon sector, where the magnetopause location requires such flows. In the simulation with vortices, the flows outside of ~15 R_S are outward throughout the region plotted. *Kivelson and Jia* [2014] have shown that the rotating system of field-aligned current incorporated in this simulation produces outward-propagating pressure pulses. The pressure pulses cause the morning side of the magnetopause to move significantly outward for a large part of each rotation period. They suggest that the outward displacement may be linked to the appearance of a flux rope in the magnetotail once each rotation. This average outward motion is captured in the plot of the radial component of the flow in the outer magnetosphere. The fact that the outward flow in the outer part of the morning sector is absent in the simulation without vortex supports the interpretation provided by *Kivelson and Jia* [2014].

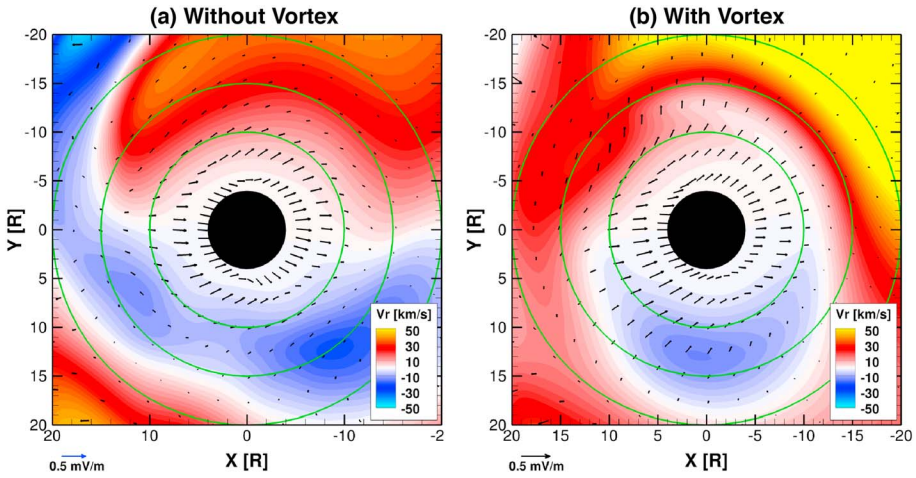

Figure 8. In color: the radial component of the flow velocity (km/s) in the equatorial plane (the Sun is to the left). (a) The image labeled without vortex is extracted from the simulation of *Jia et al*. [2012a]. (b) The image labeled with vortex is extracted from the simulation of *Jia et al*. [2012b] that includes rotating field-aligned current driven from the southern ionosphere. In both cases the simulation parameters are averaged over five rotation periods. Arrows show the direction and intensity of the $-\mathbf{v}\times\mathbf{B}$ electric field after removing the radial electric field associated with the azimuthal plasma flow, and the reference scale is shown at the bottom. Green circles have radii of 10, 15, and 20 R_S.

6. The Global Electric Field: Comparison With Observations

As previously noted, comprehensive data from the Cassini spacecraft have been used in several analyses of the global electric field. (A radially oriented electric field associated with the azimuthal flow is present in addition to the perturbation electric field on which we focus.) The field magnitude and orientation were inferred from the displacement of "microsignatures" of satellites in energetic particle fluxes [e.g., *Paranicas et al*., 2005; *Roussos et al*., 2005; *Andriopoulou et al*., 2012, 2014], from the local time asymmetry of ring absorption signatures in energetic particle fluxes [*Paranicas et al*., 2010], from the day-night asymmetries of low-energy ion and electron temperatures and the phase-space densities of energetic ions and electrons [*Thomsen et al*., 2012], and from the local time dependence of plasma radial velocities [*Wilson et al*., 2013]. In all cases, the magnitude of the convection electric field was found to be of order ~0.1 mV/m to ~0.3 mV/m and on average to point from postnoon to postmidnight. The simulation yields flow magnitudes close to 2.5 km/s, decreasing slightly with radial distance from 9 to 5 R_S, close to the values found by *Andriopoulou et al*. [2012] but lower than the values reported by *Wilson et al*. [2013] (see their Figure 8).

The electric field orientation in Figure 10 of *Wilson et al*. [2013] is close to the direction shown in the simulation with vortex in Figure 8. The slight twist toward 01 LT is less apparent in the simulation without vortex, but the strongest fields at 7.5 R_S do have a net rotation from midnight in the sense observed. In both simulations, the magnitude of the electric field in the inner magnetosphere falls in the range reported from observations.

7. Discussion and Summary

The simulated plasma and field properties of the near-equatorial regions between $L = 5$ and 10 reproduce the published results on flows and electric field to within the differences in the values reported by different observers. Analysis of two simulations provides an interpretation of the net flow from dusk to dawn. The plasma distribution along flux tubes rotating through the dayside magnetosphere is controlled by the balance of the centripetal term and the pressure gradient force. In the morning quadrant, the field is stretched by both pressure gradient and centripetal terms. The field-aligned component of the centripetal term is large, and the plasma is confined near the equator, producing a thin plasma sheet. As the plasma rotates through the morning sector, the flux tubes dipolarize in response to the inward $\mathbf{j}\times\mathbf{B}$ force. This reduces the effect of the centripetal term, and the plasma expands along the flux tube. If the pressure gradient force parallel to **B** acted alone, expansion would occur at the sound speed, a speed high enough to allow the plasma to move many R_S along the flux tube as it rotates to noon. The expansion rate is reduced by the confining effects of the centripetal term, but plasma moves away from the equator at a significant fraction of the sound speed. The

plasma sheet becomes thick. As the plasma continues to rotate beyond noon, one might expect the plasma to return to the equator and the flux tubes to become stretched, but that does not happen because the field-aligned component of the centripetal term is small near the equator in a dipolar geometry. We find that the maximum displacement through centripetal acceleration acting for about 2 h is less than half the displacement possible if plasma moves at the sound speed. With a thick plasma sheet and a quasi-dipolar field configuration, the inward $\mathbf{j} \times \mathbf{B}$ force dominates the outward centripetal term in the middle magnetosphere in the afternoon sector. Thus, the radial component of the plasma flow is inward postnoon. The simulated flow velocity is of the order of that reported from data analyses and implies an electric field of the right magnitude and an orientation close to noon-midnight, with a tendency to point a bit dawnward of midnight.

The processes that account for the configuration of Saturn's magnetosphere, especially its morning-afternoon asymmetries, are likely to be relevant to the Jovian magnetosphere as well. Jupiter's postnoon plasma sheet is known to be thicker than its prenoon plasma sheet, and its field configuration is known to be more dipolar; the differing nature of plasma expansion prenoon and contraction postnoon must play a role at Jupiter as it does at Saturn.

One is tempted to ask whether there is a noon-midnight component of the electric field in Jupiter's middle magnetosphere as there is at Saturn. It is worth noting that the orientation of Jupiter's electric field is not firmly established. Earth-based observations of the dawn-dusk asymmetry of the intensity of ultraviolet emissions from the Io plasma torus establish the presence of a finite component of the electric field in the dawn-dusk direction. However, the existence of a dawn-dusk asymmetry of intensity tells us nothing about the component of the electric field along the line of sight. A noon-midnight component of the electric field would create noon-midnight asymmetry in UV images, but such asymmetry cannot be detected from Earth [*Thomas*, 1993]. There is, however, some evidence of a component of the electric field oriented from day to night. Voyager 1 identified day-night asymmetries in the flux of energetic particles measured inbound (dayside) and outbound (nightside) on the same magnetic shell [*Cheng et al.*, 1984]. *Cheng et al.* [1984] suggested a noon-midnight component of the electric field comparable in magnitude to the nominal dawn-dusk component as one way to account for their measurements. If this field component were present, the total field would point somewhere between dusk and midnight, differing by only a few hours of local time from the orientation identified at Saturn. It is, however, also possible that the day-night asymmetry reported from the Voyager measurements may have resulted from the well-studied temporal and azimuthal variability of the Io plasma torus [*Steffl et al.*, 2006, 2008] and that available data are too sparse to establish the average electric field orientation.

Acknowledgments

We thank Tamas Gombosi for establishing a powerful computational framework without which this work could not have been undertaken and David Southwood for extremely useful comments. The authors would also like to thank the two reviewers for their constructive reviews. This work was supported by NASA through grants NNX12AK34G at the University of Michigan (X.J. and M.G.K.) and NNX13AL05G, NNX13AG87G at UCLA (M.G.K.) and by the Cassini mission under contracts JPL 1409449 (X.J.) and 1416974 (M.G.K.). Data used in this study were obtained from simulations using the SWMF/BATSRUS code developed at the University of Michigan, which is available at http://csem.engin.umich.edu/tools/swmf/. The simulation presented in this study was performed on the Pleiades supercomputer managed by the NASA Advanced Supercomputing Division.

References

Andrews, D. J., E. J. Bunce, S. W. H. Cowley, M. K. Dougherty, G. Provan, and D. J. Southwood (2008), Planetary period oscillations in Saturn's magnetosphere: Phase relation of equatorial magnetic field oscillations and Saturn kilometric radiation modulation, *J. Geophys. Res.*, *113*, A09205, doi:10.1029/2007JA012937.

Andriopoulou, M., E. Roussos, N. Krupp, C. Paranicas, M. Thomsen, S. Krimigis, M. K. Dougherty, and K.-H. Glassmeier (2012), A noon-to-midnight electric field and nightside dynamics in Saturn's inner magnetosphere, using microsignature observations, *Icarus*, *220*, 503–513, doi:10.1016/j.icarus.2012.05.010.

Andriopoulou, M., E. Roussos, N. Krupp, C. Paranicas, M. Thomsen, S. Krimigis, M. K. Dougherty, and K.-H. Glassmeier (2014), Spatial and temporal dependence of the convective electric field in Saturn's inner magnetosphere, *Icarus*, *229*, 57–70, doi:10.1016/j.icarus.2013.10.028.

Arridge, C. A., M. Kane, N. Sergis, K. K. Khurana, and C. M. Jackman (2015), Sources of local time asymmetries in magnetodiscs, *Space Sci. Rev.*, *187*, 301–333, doi:10.1007/s11214-015-0145-z.

Barbosa, D. D., and M. G. Kivelson (1983), Dawn-dusk electric field asymmetry of the Io plasma torus, *Geophys. Res. Lett.*, *10*, 210–213, doi:10.1029/GL010i003p00210.

Cheng, A. F., M. T. Paoness, C. G. Maclennan, L. J. Lanzerotti, and T. P. Armstrong (1984), Longitudinal asymmetry in the Io plasma torus, *J. Geophys. Res.*, *89*, 3005–3010, doi:10.1029/JA089iA05p03005.

Delamere, P. A., R. J. Wilson, S. Eriksson, and F. Bagenal (2013), Magnetic signatures of Kelvin-Helmholtz vortices on Saturn's magnetopause: Global survey, *J. Geophys. Res. Space Physics*, *118*, 393–404, doi:10.1029/2012JA018197.

Desroche, M., F. Bagenal, P. A. Delamere, and N. Erkaev (2012), Conditions at the expanded Jovian magnetopause and implications for the solar wind interaction, *J. Geophys. Res.*, *117*, A07202, doi:10.1029/2012JA017621.

Desroche, M., F. Bagenal, P. A. Delamere, and N. Erkaev (2013), Conditions at the magnetopause of Saturn and implications for the solar wind interaction, *J. Geophys. Res. Space Physics*, *118*, 3087–3095, doi:10.1002/jgra.50294.

Fukazawa, K., T. Ogino, and R. J. Walker (2005), Dynamics of the Jovian magnetosphere for northward interplanetary magnetic field (IMF), *Geophys. Res. Lett.*, *32*, l03202, doi:10.1029/2004GL021392.

Galopeau, P. H. M., and A. Lecacheux (2000), Variations of Saturn's radio rotation period measured at kilometer wavelengths, *J. Geophys. Res.*, *105*, 13,089–13,102, doi:10.1029/1999JA005089.

Gombosi, T. I., G. Tóth, D. L. de Zeeuw, K. C. Hansen, K. Kabin, and K. G. Powell (2002), Semi-relativistic magnetohydrodynamics and physics-based convergence acceleration, *J. Comput. Phys.*, *177*, 176–205, doi:10.1006/jcph.2002.7009.

Gurnett, D. A., et al. (2005), Radio and plasma wave observations at Saturn from Cassini's approach and first orbit, *Science*, *307*, 1255–1259, doi:10.1126/science.1105356.

Hansen, K. C., A. J. Ridley, G. B. Hospodarsky, N. Achilleos, M. K. Dougherty, T. I. Gombosi, and G. Tóth (2005), Global MHD simulations of Saturn's magnetosphere at the time of Cassini approach, *Geophys. Res. Lett.*, *32*, L20S06, doi:10.1029/2005GL022835.

Hill, T. W., A. J. Dessler, and F. C. Michel (1974), Configuration of the Jovian magnetosphere, *Geophys. Res. Lett.*, *1*, 3–6, doi:10.1029/GL001i001p00003.

Holmberg, M. K. G., J.-E. Wahlund, M. W. Morooka, and A. M. Persoon (2012), Ion densities and velocities in the inner plasma torus of Saturn, *Planet. Space Sci.*, *73*, 151–160.

Ip, W.-H., and C. K. Goertz (1983), An interpretation of the dawn–dusk asymmetry of UV emission from the Io plasma torus, *Nature*, *302*, 232–233, doi:10.1038/302232a0.

Jia, X., and M. G. Kivelson (2012), Driving Saturn's magnetospheric periodicities from the upper atmosphere/ionosphere: Magnetotail response to dual sources, *J. Geophys. Res.*, *117*, A11219, doi:10.1029/2012JA018183.

Jia, X., K. C. Hansen, T. I. Gombosi, M. G. Kivelson, G. Tóth, D. L. DeZeeuw, and A. J. Ridley (2012a), Magnetospheric configuration and dynamics of Saturn's magnetosphere: A global MHD simulation, *J. Geophys. Res.*, *117*, A05225, doi:10.1029/2012JA017575.

Jia, X., M. G. Kivelson, and T. I. Gombosi (2012b), Driving Saturn's magnetospheric periodicities from the upper atmosphere/ionosphere, *J. Geophys. Res.*, *117*, A04215, doi:10.1029/2011JA017367.

Kane, M., D. G. Mitchell, J. F. Carbary, and S. M. Krimigis (2014), Plasma convection in the nightside magnetosphere of Saturn determined from energetic ion anisotropies, *Planet. Space Sci.*, *91*, 1–13.

Khurana, K. K., M. G. Kivelson, V. M. Vasyliunas, N. Krupp, J. Woch, A. Lagg, B. H. Mauk, and W. S. Kurth (2004), The configuration of Jupiter's magnetosphere, in *Jupiter, The Planet, Satellites, and Magnetosphere*, edited by F. Bagenal et al., Cambridge Univ. Press, N. Y.

Kivelson, M. G., and X. Jia (2014), Control of periodic variations in Saturn's magnetosphere by compressional waves, *J. Geophys. Res. Space Physics*, *119*, 8030–8045, doi:10.1002/2014JA020258.

Kivelson, M. G., and D. J. Southwood (2005), Dynamical consequences of two modes of centrifugal instability in Jupiter's outer magnetosphere, *J. Geophys. Res.*, *110*, A12209, doi:10.1029/2005JA011176.

Krupp, N., A. Lagg, S. Livi, B. Wilken, J. Woch, E. C. Roelof, and D. J. Williams (2001), Global flows of energetic ions in Jupiter's equatorial plane: First-order approximation, *J. Geophys. Res.*, *106*, 26,017–26,032, doi:10.1029/2000JA900138.

Kurth, W. S., A. Lecacheux, T. F. Averkamp, J. B. Groene, and D. A. Gurnett (2007), A Saturnian longitude system based on a variable kilometric radiation period, *Geophys. Res. Lett.*, *34*, L02201, doi:10.1029/2006GL028336.

Kurth, W. S., T. F. Averkamp, D. A. Gurnett, J. B. Groene, and A. Lecacheux (2008), An update to a Saturnian longitude system based on kilometric radio emissions, *J. Geophys. Res.*, *113*, A05222, doi:10.1029/2007JA012861.

Lamy, L. (2011), Variability of southern and northern periodicities of Saturn Kilometric Radiation, in *Planetary Radio Emissions VII: Proceedings of the Seventh International Workshop, Graz, Austria, Sept 15–17, 2010*, edited by H. O. Rucker et al., pp. 39, Austrian Acad. of Sci. Press, Vienna.

Lanzerotti, L. J., et al. (1992), Measurements of hot plasmas in the magnetosphere of Jupiter, *Planet. Space Sci.*, *41*, 893.

Lecacheux, A., P. Galopeau, and M. Aubier (1997), Re-visiting Saturnian radiation with Ulysses/URAP, in *Planetary Radio Emissions IV*, edited by H. O. Rucker, S. J. Bauer, and A. Lecacheux, pp. 313–325, Austrian Acad. of Sci. Press, Vienna.

Mauk, B. H., and S. M. Krimigis (1987), Radial force balance within Jupiter's dayside magnetosphere, *J. Geophys. Res.*, *92*, 9931–41, doi:10.1029/JA092iA09p09931.

Mauk, B. H., S. M. Krimigis, and R. P. Lepping (1985), Particle and field stress balance within a planetary magnetosphere, *J. Geophys. Res.*, *90*, 8253–8264, doi:10.1029/JA090iA09p08253.

Paranicas, C., D. G. Mitchell, S. Livi, S. M. Krimigis, E. Roussos, N. Krupp, J. Woch, A. Lagg, J. Saur, and F. S. Turner (2005), Evidence of Enceladus and Tethys microsignatures, *Geophys. Res. Lett.*, *32*, L20101, doi:10.1029/2005GL024072.

Paranicas, C., D. G. Mitchell, S. M. Krimigis, J. F. Carbary, P. C. Brandt, F. S. Turner, E. Roussos, N. Krupp, M. G. Kivelson, and K. K. Khurana (2010), Asymmetries in Saturn's radiation belts, *J. Geophys. Res.*, *115*, A07216, doi:10.1029/2009JA014971.

Pilkington, N. M., N. Achilleos, C. S. Arridge, P. Guio, A. Masters, L. C. Ray, N. Sergis, M. F. Thomsen, A. J. Coates, and M. K. Dougherty (2015), Asymmetries observed in Saturn's magnetopause geometry, *Geophy. Res. Lett.*, *42*, 6890–6898, doi:10.1002/2015GL065477.

Powell, K. G., P. L. Roe, T. J. Linde, T. I. Gombosi, and D. L. DeZeeuw (1999), A solution-adaptive upwind scheme for ideal magnetohydrodynamics, *J. Comput. Phys.*, *154*, 284–309, doi:10.1006/jcph.1999.6299.

Richardson, J. D., A. Eviatar, M. A. McGrath, and V. M. Vasyliunas (1998), OH in Saturn's magnetosphere: Observations and implications, *J. Geophys. Res.*, *103*, 20,245–20,255, doi:10.1029/98JE01127.

Ridley, A., T. I. Gombosi, and D. DeZeeuw (2004), Ionospheric control of the magnetosphere: Conductance, *Ann. Geophys.*, *22*, 567–584, doi:10.5194/angeo-22-567-2004.

Roussos, E., et al. (2005), Low energy electron microsignatures at the orbit of Tethys: Cassini MIMI/LEMMS observations, *Geophys. Res. Lett.*, *32*, L24107, doi:10.1029/2005GL024084.

Sakai, S., S. Watanabe, M. W. Morooka, M. K. G. Holmberg, J.-E. Wahlund, D. A. Gurnett, and W. S. Kurth (2013), Dust–plasma interaction through magnetosphere–ionosphere coupling in Saturn's plasma disk, *Planet. Space Sci.*, *75*, 11–16, doi:10.1016/j.pss.2012.11.003.

Southwood, D. J., and M. G. Kivelson (2007), Saturnian magnetospheric dynamics: Elucidation of a camshaft model, *J. Geophys. Res.*, *112*, A12222, doi:10.1029/2007JA012254.

Steffl, A. J., P. A. Delamere, and F. Bagenal (2006), Cassini UVIS observations of the Io plasma torus. III Observations of temporal and azimuthal variability, *Icarus*, *180*, 124–140.

Steffl, A. J., P. A. Delamere, and F. Bagenal (2008), Cassini UVIS observations of the Io plasma torus. IV Modeling temporal and azimuthal variability, *Icarus*, *194*, 153–165.

Thomas, N. (1993), The variability of the Io plasma torus, *J. Geophys. Res.*, *98*(E10), 18,737–18,750, doi:10.1029/93JE01461.

Thomsen, M. F., D. B. Reisenfeld, D. M. Delapp, R. L. Tokar, D. T. Young, F. J. Crary, E. C. Sittler, M. A. McGraw, and J. D. Williams (2010), Survey of ion plasma parameters in Saturn's magnetosphere, *J. Geophys. Res.*, *115*, A10220, doi:10.1029/2010JA015267.

Thomsen, M. F., E. Roussos, M. Andriopoulou, P. Kollmann, C. S. Arridge, C. P. Paranicas, D. A. Gurnett, R. L. Powell, R. L. Tokar, and D. T. Young (2012), Saturn's inner magnetospheric convection pattern: Further evidence, *J. Geophys. Res.*, *117*, A09208, doi:10.1029/2011JA017482.

Toth, G., et al. (2012), Adaptive numerical algorithms in space weather modeling, *J. Comput. Phys.*, *231*, 870–903, doi:10.1016/j.jcp.2011.02.006.

Vogt, M., M. G. Kivelson, K. K. Khurana, R. J. Walker, and M. Ashour-Abdalla (2014), Simulating the effect of centrifugal forces in Jupiter's magnetosphere, *J. Geophys. Res. Space Physics*, *119*, 1925–1950, doi:10.1002/2013JA019381.

Wilson, R. J., R. L. Tokar, and M. G. Henderson (2009), Thermal ion flow in Saturn's inner magnetosphere measured by the Cassini plasma spectrometer: A signature of the Enceladus torus?, *Geophys. Res. Lett.*, *36*, L23104, doi:10.1029/2009GL040225.

Wilson, R. J., F. Bagenal, P. A. Delamere, M. Desroche, B. L. Fleshman, and V. Dols (2013), Evidence from radial velocity measurements of a global electric field in Saturn's inner magnetosphere, *J. Geophys. Res. Space Physics*, *118*, 2122–2132, doi:10.1002/jgra.50251.